THE PUBLISHING HOUSE
OF THE ROMANIAN ACADEMY

PROCEEDINGS OF THE ROMANIAN ACADEMY, Series A,
Volume 14, Number 4/2013, pp. 326–334

UPDATING OF AN EXHAUST SYSTEM MODEL BY USING TEST DATA FROM EMA

Iulian LUPEA

Technical University of Cluj-Napoca,
E-mail: i_lupea@yahoo.com

In the present paper the dynamics of an exhaust system is under observation. The exhaust system is modeled by using finite elements. Some differences between the CAD model and the real structure, which has been measured nondestructively, are expected. The natural frequencies, the modal vectors and the associated modal strain energy density of the structure, are observed. Then, the experimental modal analysis (EMA) of the exhaust system suspended in elastic cords has been performed. The modal parameters, derived from finite element modal analysis and experimental modal analysis, are compared. In an optimization process the mass distribution and thickness values of some parts of the finite element model are improved by matching the eigenvalues from the simulated modal analysis and EMA. This approach is a good calibration of the exhaust system model and a prerequisite for the hangers parameters optimization in the effort to minimize the transferred forces to the chassis.

Key words: exhaust system, modal analysis simulation, experimental modal analysis, size optimization.

1. INTRODUCTION

The exhaust system is mainly composed of a catalyst or catalytic converter and two acoustic volumes or mufflers, the intermediate or pre-silencer and the rear or main silencer. These functional components are interconnected by pipes. The system is connected to the manifold often by a flexible joint and to the car body by hangers. Finding the best hanging locations and characteristics can be seen as an optimization problem.

The catalyst is connected often to the manifold by a flexible joint which has a nonlinear behavior. The joint allows the motion of the engine and filters the vibration transmitted to the exhaust system.

In order to describe the dynamical behavior of the exhaust system, a dynamical simulation by using finite elements has to be performed. In parallel, the experimental approach is aiming to validate the finite element model. Considering the excitation of the system coming from the engine and the road [6], a dynamic response of the exhaust system has to be observed. The system vibration generates forces which are transmitted to the car body through the attaching or hanging points. The vibration transmitted to the car body will induce structure born noise in the cabin, as well. Hence, a plan to decouple the exhaust system vibration from the car structure is of interest. Further, the validated model can be used for optimization of the dynamical response of the whole structure. Numerous studies on the exhaust system dynamics, simulation and experiment are available in the literature [2, 7, 8, 12].

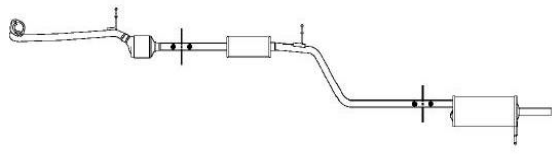

Fig. 1 – Exhaust system layout.

A physical exhaust system of Dacia Logan, has been measured accepting some approximations, which have to be overcome. Based on the geometrical or CAD model (Fig. 1), the finite element model of the whole exhaust system is developed. The normal modal analysis and the EMA are set up resulting the estimated and respectively measured system modal parameters.

2. THE FINITE ELEMENT MODEL

Starting from the surfaces of the geometry, the mesh, mainly based on shell elements, has been done. The first portion of the structure, is represented by the (hot) pipe connecting the manifold to the catalyst, a short hanger welded to the pipe and the catalyst. The catalyst and the intermediate muffler mesh is shown in Fig. 2. After a large elbow of the main pipe, on the rear portion of the structure, the gases are transferred to the main muffler and finally to the tail pipe. The interior structure and the associated cavities of the main muffler are shown in Fig. 3. The rear hanger bar is welded to the main muffler and meshed by using solid elements. In order to preserve the structural mass, of about 12.29 kg, the density of the shell elements of the catalytic converter and intermediate muffler have been properly altered.

Fig. 2 – Intermediary muffler's and catalyst's hulls.

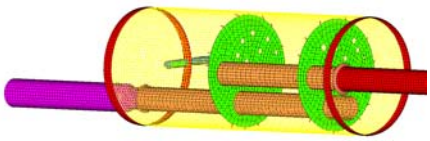

Fig. 3 – Main muffler mesh and the tail.

3. MODAL ANALYSIS - SIMULATION

3.1. The eigenvalue problem

The dynamical equations of mechanical systems with linear behavior, can be written in matrix form, as follows: $\mathbf{M}\ddot{\mathbf{Q}} + \mathbf{D}\dot{\mathbf{Q}} + \mathbf{K}\mathbf{Q} = \mathbf{F}$, where $\mathbf{Q}$ is the vector of the system generalized coordinates or system degrees of freedom, $\mathbf{M}$, $\mathbf{D}$, $\mathbf{K}$ are the mass (inertia), viscous assumed damping and stiffness matrices and F is the vector of generalized forces. The matrices $\mathbf{M}$, $\mathbf{D}$ and $\mathbf{K}$ are considered symmetrical, with $n \times n$ elements. When doing the normal mode analysis of the system, the damping is neglected and the external forces are not acting, resulting equation: $\mathbf{M}\ddot{\mathbf{Q}} + \mathbf{K}\mathbf{Q} = 0$. Assuming a harmonic and synchronous motion in the structure, when all coordinates perform in time the motion in phase or out of phase, the following solution is proposed: $\mathbf{Q}(t) = \mathbf{u} \cdot \cos(\omega t - \varphi)$, where ω is considered the natural frequency of the whole system and $\mathbf{u}$ is a constant n–vector of amplitudes. By replacing the proposed solution in the system of differential equations, results:

$$\mathbf{K}\mathbf{u} - \omega^2\mathbf{M}\mathbf{u} = 0 \text{ or } (\mathbf{K} - \omega^2\mathbf{M}) \cdot \mathbf{u} = 0. \tag{1}$$

The resulted set of homogeneous algebraic equations has the unknown vector $\mathbf{u}$. Considering $\lambda = \omega^2$ as a parameter, one gets: $\mathbf{K}\mathbf{u} = \lambda\mathbf{M}\mathbf{u}$ known as the eigenvalue problem when trying to determine λ values for which the system has nontrivial solutions for $\boldsymbol{u}$. By solving with respect to λ and nontrivial solution, the following characteristic equation, is obtained: $\det(\mathbf{K} - \lambda\mathbf{M}) = 0$, where λ_r (r = 1,2...,n) values are the eigenvalues (characteristic values) of the system. The natural frequencies of the system are derived:

$$f_r = \sqrt{\lambda_r} / 2\pi \quad r = 1, 2, ...n. \tag{2}$$

For each determined eigenvalue λ_r, an eigenvector $\boldsymbol{u}_r$ (r = 1,2...,n) defining the associated mode shape of vibration, is satisfying the equation: $\mathbf{K}\mathbf{u}_r = \lambda_r\mathbf{M}\mathbf{u}_r \quad r = 1, 2, ..., n$. This general approach is implemented in commercial solvers and by using various numerical algorithms, like the Lantzos algorithm implemented in Optistruct solver [15], the normal modal analysis of a system is performed.

3.2. Modal analysis simulation: eigenvalues, mode shapes and strain energy density

A modal analysis (MA) simulation of the structure free of constraints, has been performed by using finite element analysis. The results are natural frequencies f_r, eigenvalues λ_r and eigenvectors $\boldsymbol{u}_r$. Associated

to each vibration mode, one can observe the displacement vector, the animation and the strain energy density for the entire structure. The first twelve natural frequencies are listed in Table 1.

In mode #1, the structure is bending like a beam with two nodes located around the catalyst and the main muffler. The mode is approximately moving in the horizontal plane (Fig. 4). In mode #2 the system is bending in a perpendicular plane comparing to the first mode and like a beam with two nodes. The first mode, in isometric views, is shown in Fig. 4. For the second mode, the deformed versus undeformed shapes and the contour plot of the deformation amplitude for the entire structure, can be seen in Fig. 5. For the first two modes the strain energy density is larger at the two corners of the pipe between the main muffler and the intermediate muffler

The most important strain energy density zones for the second mode of vibration are depicted in Fig. 6. The third mode presents three nodes and the main movement is in horizontal plane (Fig. 7). The strain energy density, sed, for a generalized state of stress and a linear elastic material is calculated following the relation (3):

$$\text{sed} = \tfrac{1}{2}(\sigma_x \varepsilon_x + \sigma_y \varepsilon_y + \sigma_z \varepsilon_z + \tau_{xy}\gamma_{xy} + \tau_{yz}\gamma_{yz} + \tau_{xz}\gamma_{xz}), \quad (2)$$

where the normal and shear stresses and strains are present. Modal strain energy density or the strain energy per unit volume, is showing the areas of the structure the most labored for each mode of vibration. In a similar manner the rest of the modes up to the 12th mode, are observed.

Table 1

Mode no.	FEA [Hz] (MA)
1	9.13
2	10.6
3	24.4
4	26.4
5	34.7
6	48.7
7	52.7
8	62
9	71
10	88.6
11	114.2
12	128.8

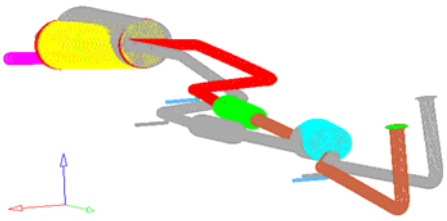

Fig. 4 – Mode #1 deformed vs. undeformed.

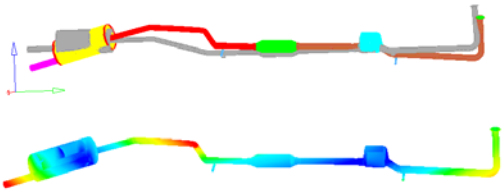

Fig. 5 – Mode of vibration #2.

Fig. 6 – Strain energy density, mode #2.

Fig. 7 – Mode #3, upper view, three nodes.

4. EXPERIMENTAL MODAL ANALYSIS IN FREE OF CONSTRAINTS CONDITIONS

Experimental modal analysis (EMA) is the process of extracting modal parameters of a mechanical structure starting from vibration data measured on the structure [9, 11, 13, 14]. When the frequency response functions (FRFs) are used, the extraction process is called frequency response domain analysis. FRF is a description of the input-output relationship as a function of frequency between two degrees of freedom of the structure. When the impulse response functions (IRFs) are used, the approach is called time domain modal analysis. The mathematical model in case of frequency domain modal analysis is an analytical expression of a FRF best fitted with the measured FRFs. In reality a structure has an infinite number of DOF and poles.

Lightly damped modes have narrow peaks in frequency domain described by a few points, hence the modal parameters are not so easy to be determined. On the contrary, in time domain, the signal of the impulse response has long duration decay and is easier to be identified. Over the last years, techniques for parameter identification only from output data (input being the operational data) have been developed. One can mention Auto-Regressive Moving Averaging models (ARMA), Natural Excitation Technique (NexT), stochastic subspace methods and others [1, 14].

4.1. The measurement set-up and the modal parameters estimation

The exhaust system has been suspended on elastic cords trying to minimize the stress in the structure and to allow the rigid body modes movement. Experimental modal analysis by using impact testing has become largely known as a fast and economical mean of finding modal parameters of a structure. In this approach, the impact hammer was connected to the first channel of an LMS acquisition system (Pimento) and was used to excite the structure in 20 locations (roving hammer), first in the vertical (V) plane and secondly in the horizontal (H) plane. A Dytran mini-accelerometer of 1.5 grams is placed into the proper reference point for the vertical and later for the horizontal set of FRFs measurement. The accelerometer is connected to the second channel of the acquisition system in order to record the response of the structure.

The impact force and the acceleration have been recorded simultaneously for each pair of measuring points. A column of 19 FRFs of the transfer matrix has been built for the EMA in vertical plane and a set of 20 FRF's for the horizontal EMA, by using LMS Test.Xpress software [16]. A schematic overview of the experimental test set-up and FRF derivation is shown in Fig. 8.

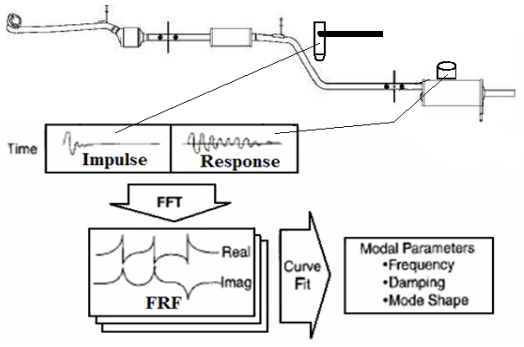

Fig. 8 – Experimental set-up.

For the parameter estimation, the LMS Test-Lab dedicated software [16], has been used. The identification process is starting from the set of 19 FRFs measured on the exhaust system. The impact locations (white labels) spread uniformly along the system, can be seen in Fig. 9. When estimating the poles, the frequency band of analysis should not be very wide. It is advisable to select several consecutive narrow bands instead of a large one in order to evaluate the parameters of the band of interest. When the estimation approach is based on a time domain technique and we are starting from FRFs, each frequency band is advisable to contain a power of two frequency lines. This will ease the conversion of data from frequency domain to time domain. In order to minimize the out of band effects the FRFs values at the limits of the band should be small (local minima).

Fig. 9 – Impact locations on the structure.

The estimation of the physical pole number can be done by counting the peaks in the FRF amplitude function. A frequently used method is to visualize the sum of the measured FRFs (amplitude) and to count the peaks. Large peaks indicate large total modal displacements, while small peaks indicate small total displacements or local modes of vibration. In general, the number of peaks will be less than the roots number, one cause being the fact that a multiple root is associated to one peak. The Mode indicator function (MIF) can help in counting the poles. The local minima of the MIFs indicate the resonances of the normal modes of the structure.

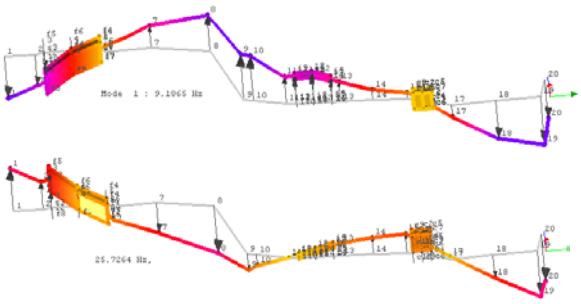

Fig. 10 – Modes #1 and #3, H plane.

A global parameter stabilization diagram for the first frequency band has been observed. The analysis is repeated for increasing model order, resulting each time a line in the diagram. The Stabilization diagram is used to bring together the poles coming from successive analysis, each analysis with a different model order. This diagram is a good tool to find the physical poles. Some of the resulting poles do not have a physical meaning. These poles are in general caused by mathematical, computational effects or noise and result from the forced fulfillment of the estimated model order, which often is larger than the model order embedded in the test

data. The physical poles tend to appear at each model order at the same frequency, which is not the case for the computational poles. The horizontal axis of the diagram registers the damped natural frequencies of the estimated poles and the vertical axis the solution order. In general the stabilization chart of LSCE method is not so clear as it is the one generated for instance by the poly-reference frequency-domain estimating procedure. After the pole selection is completed, the modal shapes are calculated by using the complex residues [16]. The first 12 complex poles, damping and damped natural frequencies are calculated.

The results are the natural frequencies, the eigenvectors and the critical damping for each vibration mode. A list of the first twelve resonant frequencies is available in Table 2. The modes quality has been checked by superposing on the measured FRFs the synthesized FRFs based on the identified modal parameters and the MAC matrix. A simplified geometry is created to visualize the measured mode shapes of the system. Two of the mode shapes are depicted in Fig. 10.

Table 2

Mode no.	EMA [Hz]	V(oz) or/and H(oy) plan better seen
1	9.19	H
2	11.74	_V
3	25.6	H
4	32.9	HV
5	38	HV
6	58.5	H
7	62.5	HV
8	75.7	HV
9	92.1	HV
10	104.6	HV
11	115.6	HV
12	128.5	HV

4.2. Aspects on the Least-square complex exponential (LSCE) parameter estimation method

LSCE method is a time domain approach which uses the impulse response functions (IRFs) of a multi degree of freedom system to estimate the complex poles and residues [1, 3, 4, 5]. Global estimates of the modal parameters are obtained since data is analysed simultaneously. The LSCE estimation is one of the most frequently used technique in industry.

In the sequel important steps of the method will be shortly presented [4, 5]. The set of FRFs is based on a matrix of typical FRFs measured between pairs (*i*-response, *j*-excitation) of generalized coordinates or degrees of freedom. Considering the influence of the first *n* modes of vibration, a typical FRF expression, has the following form:

$$H_{ij}(s) = \sum_{r=1}^{n} \left(\frac{A_{ijr}}{s - s_r} + \frac{A^*_{ijr}}{s - s_r^*} \right) \tag{4}$$

or:

$$H_{ij}(s) = \sum_{r=1}^{2n} \frac{A_{ijr}}{s - s_r}, \tag{5}$$

where for $r > n$ one have $A_{ijr} = A^*_{ijr}$ and $s_r = s^*_r$. $\boldsymbol{H}$ is the transfer function matrix of the system, $\boldsymbol{A_r}$ is the residue matrix associated to the mode *r* and s_r is the pole indices *r* of the system. The relations (4) and (5) are transformed into the IRFs by inverse Laplace transform, resulting:

$$h_{ij}(t) = \sum_{r=1}^{2n} A_{ijr} e^{s_r t} \quad \text{or} \quad h_{ij}(t) = \sum_{r=1}^{n} \left(A_{ijr} e^{s_r t} + A^*_{ijr} e^{s^*_r t} \right). \tag{6}$$

The poles s_r, being global characteristics of the structure, are not dependent of a particular (input, output) pair of locations and orientations or '*ij'* DOFs. On the contrary, the residues are dependent on the response and excitation pair '*ij'* DOFs. This aspect can be observed on the Equations (5) and (6).

IRFs are sampled at equally spaced time intervals d*t,* at the moments $k \cdot \mathrm{d}t$ (k=0,1,2,…,2n):

$$h_{ij}(k \cdot \mathrm{d}t) = \sum_{r=1}^{2n} A_{ijr} e^{s_r \cdot k \cdot \mathrm{d}t} \quad (k = 0, 1, ..., 2n). \tag{7}$$

Based on these samples (from experiment), the parameters are estimated. By considering the substitution:

$$z_r = e^{s_r \cdot \mathrm{d}t} \tag{8}$$

series of powers are resulting: $e^{s_r \cdot k \cdot dt} = (e^{s_r \cdot dt})^k = z_r^k$.

Each IRF can be split into discrete values:

$$h_{ij,k} = \sum_{r=1}^{2n} A_{ij\,r} \cdot z_r^k \quad (k = 0,1,...,2n) \tag{9}$$

or:

$$h_{ij,k} = \sum_{r=1}^{n} (A_{ij\,r} \cdot z_r^k + A_{ij\,r}^* \cdot z_r^{k\,*}) \quad (k = 0,1,...,n), \tag{9b}$$

where $h_{ij,k} = h_{ij}(k \cdot dt)$ are real values known from measurements, $A_{ij\,r}$ are the residues (complex values) and z_r^k are complex values because the poles s_r are complex. Imaginary components on the right side of the equation (9) cancel each other because the residues and the poles numbered from n+1 to 2n are the conjugates of the first *n* residues and poles. Considering that z_r are grouped in complex conjugates pairs one can assume, by using Prony's fitting method, that these pairs are the roots of a polynomial with real coefficients β_k, k=0,1,2,…,2n. For the root values the polynomial vanishes, resulting Prony's equation of the form:

$$\beta_0 + \beta_1 \cdot z_r + \beta_2 \cdot z_r^2 + ... + \beta_{2n} \cdot z_r^{2n} = 0, \text{ or } \sum_{r=0}^{2n} \beta_k \cdot z_r^k = 0. \tag{10}$$

Using the available discrete data from IRFs (measured data), the coefficients β_k of relation (10), can be estimated. In relation (9), by multiplying each equation (k = 0,1,…,2n) with the specific coefficient β_k and adding all equalities together, the relation (11) is obtained:

$$\sum_{k=0}^{2n} \beta_k h_{ij,k} = \sum_{k=0}^{2n} \beta_k \sum_{r=1}^{2n} A_{ij\,r} \cdot z_r^k. \tag{11}$$

On the right member of (11) one can interchange the summations and moving the residues $A_{ij\,r}$ out from the summation with respect to the index k:

$$\sum_{k=0}^{2n} \beta_k h_{ij,k} = \sum_{r=1}^{2n} A_{ij\,r} \cdot \sum_{k=0}^{2n} \beta_k \cdot z_r^k. \tag{12}$$

In the right side of the equation (12) we recognize the summation of the relation (10) which is zero for the set of z_r^k roots of the polynomial mentioned in relation (10). For this z_r set of values, the right member of the equation is vanishing, resulting:

$$\sum_{k=0}^{2n} \beta_k h_k = 0, \tag{13}$$

in which β_k values are not known and h_k values are known samples of IRF data (*'ij'* indices have been neglected). By setting $\beta_{2n} = -1$ and moving h_k on the right side of the equation, the relation (13) still remains valid. The rest of 2n–1 unknown coefficients can be determined. Taking 2n samples from an IRF we have one equation of type (13). Taking 2n sets of samples from IRFs we define a system of 2n linear equations from which the set of β_k (k = 0,…,2n–1) coefficients can be estimated.

$$\begin{bmatrix} h_0 & h_1 & h_2 & \cdots & h_{2n-1} \\ h_1 & h_2 & h_3 & \cdots & h_{2n} \\ \vdots & \vdots & \vdots & \cdots & \vdots \\ h_{2n-1} & h_{2n} & h_{2n+1} & \cdots & h_{4n-2} \end{bmatrix} \begin{bmatrix} \beta_0 \\ \beta_1 \\ \vdots \\ \beta_{2n-1} \end{bmatrix} = \begin{bmatrix} h_{2n} \\ h_{2n+1} \\ \vdots \\ h_{4n-1} \end{bmatrix}. \tag{14}$$

For the least square solution the number of equations in the system written in matrix form (14) can be greater than the number of unknown coefficients. The data samples h_i, n values in each row, are evenly spaced in time. Once the set of β coefficients are calculated one can solve the polynomial equation (10) for the unknown roots $z_r : \sum_{r=0}^{2n} \beta_k \cdot z_r^k = 0$. By applying the natural logarithm on relation (14), results:

$$s_r \mathrm{d}t = \ln z_r \quad \text{and} \quad s_r^* \mathrm{d}t = \ln z_r^* . \tag{15}$$

Multiplying the two equations of relation (15) one gets: $s_r s_r^* = \ln z_r \ln z_r^* / \mathrm{d}t^2$

By considering the expressions of the system poles:

$$s_r = -\zeta_r \omega_r + \mathrm{j}\sqrt{1-\zeta_r^2}\,\omega_r, \; s_r^* = -\zeta_r \omega_r - \mathrm{j}\sqrt{1-\zeta_r^2}\,\omega_r, \tag{16}$$

the natural frequency and damping ratio for each mode, can be found:

$$\omega_r = \tfrac{1}{\mathrm{d}t}\sqrt{\ln z_r \ln z_r^*}, \; \zeta_r = \frac{-\ln(z_r z_r^*)}{2\omega_r \cdot \mathrm{d}t}. \tag{17}$$

The LSCE model does not estimate the mode shapes. These are derived by the Least-Squares Frequency Domain (LSFD) method. The derivation of the system mode shapes resides in finding A_{ijr} residues for various *'ij'* degrees of freedom and '*r*' modes:

$$\begin{bmatrix} 1 & 1 & 1 & \cdots & 1 \\ z_1 & z_2 & z_3 & \cdots & z_{2n} \\ \vdots & \vdots & \vdots & \vdots & \vdots \\ z_1^{2n-1} & z_2^{2n-1} & z_3^{2n-1} & \cdots & z_{2n}^{2n-1} \end{bmatrix} \begin{bmatrix} A_{ij1} \\ A_{ij2} \\ \vdots \\ A_{ij\,2n} \end{bmatrix} = \begin{bmatrix} h_0 \\ h_1 \\ \vdots \\ h_{2n-1} \end{bmatrix}. \tag{18}$$

5. MODEL UPDATING BY SIZE OPTIMIZATION

Discrepancies on the natural frequencies values, between experimental modal analysis and modal analysis simulation by using finite elements, are observed. These are coming from the modeling uncertainties, mainly from the exhaust system CAD geometry inaccuracies and the mass and rigidity distribution errors on the simulation model. The FEM has been updated by using test data and size optimization. In order to update the model, a size optimization [10], [15] has been performed. The difference between the simulation results and test data has to be minimized. The design space is defined by considering a set of five design variables. By varying these variables the mass and stiffness distribution over the system and the associated inertial and stiffness matrices of the system can be influenced locally and/or globally. Three out of five variables are changing the wall thickness values of the sheet metal on three different areas of the structure. Two other variables are changing the density values of the catalytic converter and the intermediate muffler sheet metal enclosures, changing their mass. The list of the design variables is presented in Table 3. The design model responses are the first twelve natural frequencies, the total mass of the system, and a calculated expression/function that has to be minimized. The target of the optimization is to find a set of design variables that minimize the following expression (19):

Table 3

Design variables

No	The affected property	Initial values	Optimal values
1	Thickness: hot pipe	1.0 mm	2.08 mm
2	Thickness: cold pipe	1.0 mm	1.29 mm
3	Thickness: of main muffler sheet metal envelope	1.0 mm	0.577 mm
4	Density: catalyst sheet metal envelope	10e-9 ton/mm^3	8.9e-9 ton/mm^3
5	Density: muffler intermediate sheet metal envelope	10e-9 ton/mm^3	17.6e-9 ton/mm^3
Total Mass [tons]		Measured 0.01229	Resulted FEA 0.01212

$$\text{Expr} = \sum_i w_i \cdot \left((f_{si} - f_{Ti}) / f_{Ti} \right)^2, \; i = 1, \ldots n, \tag{19}$$

where f_{Ti} are the target natural frequencies coming from test (EMA) (Table 2), f_{si} are the natural frequencies values from simulation, n is the number of natural frequencies that have to be matched, twelve in this approach and w_i are the coefficients of importance associated to each term in the summation.

In the sequel the optimization results are presented. During the optimization process, eigenvalues are changing at each iteration, minimizing the user-written equation 'Expr' or the objective function from 0.3325 to 0.04. The first twelve modal shapes for the first iteration and the last or optimal iteration are similar, showing that the change of natural frequencies (Table 4) did not change the order of the mode shapes. Restrictions were proposed for the design variables. Some restrictions came from measurements on a similar and used part, mainly thicknesses on the main muffler and the cold pipe. The best values for final exhaust system mass (12.12kg) resulted when unconstrained design variables (three thickness values and two density values) and the mass response have been proposed. For a list of different starting values for the design variables, the minimal value of the objective function is the same of 0.04. The new or optimal thickness values and the resulted densities (Table 3) are applied to the finite element model.

Table 4

Optimal eigenvalues

Mode #	(EMA) eigval.	Final eigval.
1	9.19	9.54
2	11.74	11.56
3	25.6	28.61
4	33	30.62
5	38	41.11
6	58.5	52.64
7	62.5	59.52
8	75.7	74.9
9	92.1	91.17
10	104.6	106.68
11	115.6	115.3
12	128.5	126.3
Expr: from 0.3325 to 0.04		
Mass response after optimization = 0.01212 tons		
Mass error after optimization (12.12–12.29)/12.29 = > 1.3%		

6. CONCLUSIONS

In the present study, the exhaust system of a car has been considered for modal parameters identification. The CAD of the real exhaust system has been built based on nondestructive measurements and the finite element model has been developed. A couple thickness values and the masses of the intermediate muffler and the catalyst at the beginning are assumed and not exactly known. In the first stage the modal analysis of the free of constraints finite element model of the system reveled with approximation the eigenvalues and the mode shapes. The experimental modal analysis of the exhaust system suspended on elastic cords has been performed. The experimental modal parameters set has been determined including the modal damping. Starting from the two sets of modal parameters a successfully size optimization has been performed. By changing thickness and density values of the proper components of the finite element model, the objective function expressing the difference between the measured and the simulated first twelve resonant frequencies, has been minimized. The optimal values have been considered in the simulation model for further processing. This approach is a good calibration of the exhaust system finite element model in order to have a correct dynamic response to excitations. It is a prerequisite for optimization of the hanger's parameters in the effort of minimizing the transferred forces from the exhaust system to the chassis.

REFERENCES

1. Brown, D., Allemang, R., Zimmerman, R., and Mergeay M., *Parameter estimation techniques for modal analysis*, SAE Paper, No. 790221. 1979.
2. Englund, T., Wall, J., Ahlin, K. and Broman, G., *Significance of non-linearity and component-internal vibrations in an exhaust system*; http://www.wseas.us/e-library/conferences/skiathos 2002/ papers, 2002.
3. Guillaume, P., Verboven, P., Vanlanduit, S., Auweraer, H. and Peeters, B. *A poly-reference implementation of the least-squares complex frequency-domain estimator*; http://sem-proceedings.com/21i/ sem.org- IMAC-XXI-Conf-s39p02.
4. He, J. and Fu, Z.F., *Modal analysis*, Butterworth Heineman, Oxford, 2001.
5. Heylen, W., Lammens, S. and Sas P., *Modal Analysis Theory and Testing*, Leuven, Katholieke Universteit Leuven, Department Werktuigkunde, 2007.
6. Lak, M., Degrande, G., Lombaert, G., *The effect of road unevenness on the dynamic vehicle response and ground-borne vibrations due to road traffic*, Soil Dynamics and Earthquake Engineering, **31**, pp. 1357–1377, 2011.

7. Lauwagie, T., Strobbe, J., Dascotte, E., Clavier, J. and Monteagudo, M., *Optimization of the dynamic response of a Complete Exhaust System,* Proceedings of the IMAC-XXVII, Feb. 9-12, 2009, Orlando, Florida (USA), Society for Experimental Mechanics Inc., 2009.
8. Li, S.,B., Guan, X., Lu, T. and Zhang, J., *Vehicle modeling with the exhaust system and experimental validation to investigate the exhaust vertical vibration characteristics excited by road surface inputs*, Int. J. Automotive Technology, **9**, *4*, 483–491,2008
9. Lupea, I., *On the modal analysis of a robot*, Proceedings 5th International Workshop on Robotics in Alpe-Adria -Danube Region RAAD'96, June 10–12, Budapest, 1996, pp. 309–313.
10. Lupea, I., Cormier, J., *Size And Shape Optimization of a Polymeric Impact Energy Absorber By Simulation*, Materiale Plastice, **44**, *4*, 339-344, 2007.
11. Maia, N.M.M. and Silva, J.M.M. (editors), *Theory and Experimental Modal Analysis*, Research Studies Press LTD, 2000.
12. Wall, J., Englund, T., Ahlin, K. and Broman, G., *Modeling of multiple bellows flexible joints of variable mean radius*, Proc. of the NAFEMS World Congress, Orlando USA, 2003.
13. Yang, C., Adams, D., Yo, S. and Kim, H*., An embedded sensitivity approach for diagnosing system-level vibration problems*, Journal of Sound and Vibration, **269**, pp. 1063–1081, 2004.
14. Zhou, W. and Chelidze, D., *Generalized Eigenvalue Decomposition in Time Domain Modal Parameter Identification*, Journal of Vibration and Acoustics, **130**, 011001-1, 2008.
15. *** HyperWorks-Optistruct, Altair Engineering, Troy, MI, USA, 2008.
16. *** TestExpress and TestLab (2008), LMS International, Leuven, Belgium, 2008.

Received February 20, 2013